

Environmental Effects on the Terahertz Surface Plasmons in Epitaxial Graphene

Godfrey Gumbs¹, Andrii Iurov², Jhao-Ying Wu³, M. F. Lin³, Paula Fekete⁴

¹*Department of Physics and Astronomy
Hunter College of the City University of New York
695 Park Avenue, New York, NY 10065 USA*

²*Center for High Technology Materials,
University of New Mexico,
Albuquerque, New Mexico, 87106, USA*

³*Department of Physics,
National Cheng Kung University, Tainan, Taiwan 701*

⁴*US Military Academy, West Point, NY*

In this paper, we predict the existence of low-frequency nonlocal plasmon excitations at the vacuum-surface interface of a superlattice of N graphene layers interacting with a thick conducting substrate. This is different from graphite which allows inter-layer hopping. A dispersion function is derived which incorporates the polarization function of the graphene monolayers (MLGs) and the dispersion function of a semi-infinite electron liquid at whose surface the electrons scatter specularly. We find that this surface plasmon-polariton is not damped by the particle-hole excitations (PHEs) or the bulk modes and separates below the continuum mini-band of bulk plasmon modes. For a conducting substrate with surface plasmon frequency $\omega_s = \omega_p/\sqrt{2}$, the surface plasmon frequency of the hybrid structure always lies below ω_s . The intensity of this mode depends on the distance of the graphene layers from the surface of the conductor, the energy band gap between the valence and conduction bands of MLG and, most importantly, on the number of two-dimensional (2D) layers. Furthermore, the hybrid structure has no surface plasmon for a sufficiently large number ($N \gtrsim 7$) of layers. The existence of two plasmons with different dispersion relations indicates that quasiparticles with different group velocity may coexist for various ranges of wavelength which is determined by the number of layers in the superlattice.

PACS numbers: 73.21.-b, 03.67.Lx, 71.70.Ej, 73.20.Mf, 71.45.Gm, 71.10.C

I. INTRODUCTION

Several years ago, there was considerable activity in the study of the electronic properties of layered semiconductor superlattices [1–5] leading to intriguing transport and optical properties which are the result of quantum mechanical effects on the nanoscale. Specifically, it was desirable to learn how a periodic or quasi-periodic array [6] of two-dimensional electron liquid (2DEL) layers, would lead to a modification of the response of the charge-density excitations to an electromagnetic field. Recently, there has been some investigation regarding the Coulomb excitations of an N -layered superlattice of free-standing monolayer graphene layers (MGLs) [7]. However, what was neglected in that study is the interaction between epitaxial layers of graphene and a conducting substrate which may give rise to composite plasmon-plasmon resonances. A low-frequency mode emerges below the continuum of modes in the limit of a large number of layers and is associated with the air-exposed surface of the graphene-conductor substrate combination. As a matter of fact, several authors [8–13] demonstrated how the electronic response properties of graphene-metal composites of Ru and Ni, for example, are much different from free-standing structures. Furthermore, these complex carbon/metal interfaces are interesting because of the unusual and fundamental physics regarding their electronic and magnetic properties at the 2D interfaces. Examples of these systems occur in intercalated graphite [14], incommensurate transition metal/graphene [15] and carbide/graphene interfaces [16]. Possible motivation for pursuing this area of research is the tunability of graphene plasmons by a substrate which is a promising emerging field of graphene-based plasmonics.

Here, we demonstrate how the intensity of the response of the surface plasmon arising when N graphene layers interact with a conducting substrate may be adjusted by changing the layer-substrate separation, the energy band gap or the number of 2D layers. It has been shown that such an energy gap may be produced by circularly polarized light [17, 18]. We employ our model to determine the plasmon excitation dispersion relation for a single layer on a conducting substrate and show how our results may simulate the experimental data recently reported by Politano, et al. [9–13]. Additionally, this paper investigates multi-layer graphene generally, showing how its new surface mode depends on the in-plane wave vector and the critical wave vector q_c which marks the onset of damping by bulk modes in the miniband continuum.

The model we use for a superlattice consists of N 2D graphene layers whose planes are perpendicular to the z -axis

at $z = a_1, a_2, \dots, a_N$ and the substrate occupies the half-space $z < 0$. Each graphene layer will be described by an energy band structure for Dirac fermions and may be intrinsic, gapped or doped. This model does not allow inter-layer hopping and hence it differs from the one we employed to describe the anisotropy of π -plasmon dispersion in AA-stacked graphite [19]. The screening of an externally applied frequency-dependent potential by the polarized medium requires a knowledge of the dielectric function of the structure which we obtain in the random-phase-approximation (RPA). We present our method of calculation in Sec. II. Section III is devoted to numerical results and discussion of our plasmon dispersion when several graphene layers interact with a conducting substrate. The simulated data show how the intensity of the modes depends on the number of layers which are stacked, their distance from the conducting surface as well as the energy gap. For $N = 1$ gapless MLG, when the conductor surface-MLG separation exceeds a critical distance d_c , the intensity of the surface plasmon in the long wavelength regime is sufficiently high to be observable up to some cut-off wave vector q_c of the surface plasmon frequency. Beyond q_c , the intensity of ω_c is very weak until the plasmon wave vector reaches some value q'_c . However, when the surface-MLG separation is less than d_c , the surface plasmon intensity in the long wavelength regime is weak and the mode only appears at shorter wavelengths when the in-plane wave vector $q_{||} > q'_c$. Interestingly, for gapped graphene, ω_c is completely suppressed when the surface-layer separation is less than d_c . We then make some concluding remarks in Sec. IV regarding the inspiration for our work, a summary and significance of our findings, and what new theoretical formalism is presented in our paper.

II. GENERAL FORMULATION OF THE PROBLEM

In our formalism, we consider a nano-scale system consisting of an arbitrary number of 2D layers and a thick conducting material. The layer may be monolayer graphene or a 2DEL such as a semiconductor inversion layer or HEMT (high electron mobility transistor). The graphene layer may have a gap, thereby extending the flexibility of the composite system that also incorporates a thick layer of dielectric material. The excitation spectra of allowable modes will be determined from a knowledge of the non-local dielectric function $\epsilon(\mathbf{r}, \mathbf{r}'; \omega)$ which depends on position coordinates \mathbf{r}, \mathbf{r}' and frequency ω or its inverse $K(\mathbf{r}, \mathbf{r}'; \omega)$ satisfying $\int d\mathbf{r}' K(\mathbf{r}, \mathbf{r}'; \omega) \epsilon(\mathbf{r}', \mathbf{r}''; \omega) = \delta(\mathbf{r}, \mathbf{r}'')$.

In operator notation, the dielectric function for the N 2D layers and a semi-infinite structure is given by [20]

$$\hat{\epsilon} = \hat{1} + \hat{\alpha}_{SI} + \sum_{i=1}^N \hat{\alpha}_{2D}^{(i)} \equiv \hat{\epsilon}_{SI} + \sum_{i=1}^N \hat{\alpha}_{2D}^{(i)} = \hat{K}_{SI}^{-1} + \sum_{i=1}^N \hat{\alpha}_{2D}^{(i)}, \quad (1)$$

where $\hat{\epsilon} = \hat{K}^{-1}$ with \hat{K} the inverse dielectric function satisfying

$$\hat{K} = \hat{K}_{SI} - \hat{K}_{SI} \cdot \sum_{i=1}^N \hat{\alpha}_{2D}^{(i)} \cdot \hat{K}. \quad (2)$$

In integral form, after Fourier transforming parallel to the xy -plane and suppressing the in-plane wave number $q_{||}$ and frequency ω , we obtain

$$K(z_1, z_2) = K_{SI}(z_1, z_2) - \sum_{i=1}^N \int_{-\infty}^{\infty} dz' \int_{-\infty}^{\infty} dz'' K(z_1, z') \alpha_{2D}^{(i)}(z', z'') K(z'', z_2). \quad (3)$$

Here, the polarization function for the 2D structure is given by

$$\alpha_{2D}^{(i)}(z', z'') = \int_{-\infty}^{\infty} dz''' v(z', z''') D^{(i)}(z''', z''), \quad (4)$$

where the 2D response function obeys

$$D^{(i)}(z''', z'') = \Pi_{2D,i}^{(0)}(q_{||}, \omega) \delta(z''' - a_i) \delta(z'' - a) \quad (5)$$

with $\Pi_{2D,i}^{(0)}(q_{||}, \omega)$ the single-particle in-plane response [21, 23, 24, 26]. The 2D RPA ring diagram polarization function for graphene with a gap Δ may be expressed as

$$\begin{aligned} \Pi_{2D}^{(0)}(q_{\parallel}, \omega) &= \frac{g}{4\pi^2} \int d^2\mathbf{k} \sum_{s,s'=\pm} \left(1 + ss' \frac{\mathbf{k} \cdot (\mathbf{k} + \mathbf{q}_{\parallel}) + \Delta^2}{\epsilon_k \epsilon_{|\mathbf{k}+\mathbf{q}_{\parallel}|}} \right) \\ &\times \frac{f(s\epsilon_{\mathbf{k}}) - f(s'\epsilon_{\mathbf{k}+\mathbf{q}_{\parallel}})}{s\epsilon_{\mathbf{k}_{\parallel}} - s'\epsilon_{\mathbf{k}+\mathbf{q}_{\parallel}} - \hbar\omega - i0^+}, \end{aligned} \quad (6)$$

where $g = 4$ takes account of valley and spin degeneracy. At $T = 0$, the Fermi-Dirac distribution function is reduced to the Heaviside step function $f(\epsilon, \mu; T \rightarrow 0) = \eta_+(\mu - \epsilon)$. In the long wavelength limit, the real part of $\Pi^0(q, \omega)$ is given by

$$\begin{aligned} \text{Re } \Pi_{2D}^{(0)}(q_{\parallel}, \omega) &= - \frac{q_{\parallel}^2}{4\pi\hbar^2\omega^2} \left\{ 4\mu + \hbar\omega \ln \left(\frac{2\mu - \hbar\omega}{2\mu + \hbar\omega} \right) \right\} \\ &- \frac{v_F^2 q_{\parallel}^4}{4\pi} \left\{ \frac{3\mu}{\hbar^2\omega^4} - \frac{\mu\hbar^2}{4\mu^2 - \hbar^2\omega^2} + \frac{1}{2\hbar\omega^3} \ln \left(\frac{2\mu - \hbar\omega}{2\mu + \hbar\omega} \right) \right\}, \end{aligned} \quad (7)$$

and the imaginary part by

$$\text{Im } \Pi_{2D}^{(0)}(q_{\parallel}, \omega) = \frac{q_{\parallel}^2}{4\hbar\omega} \left(1 + \frac{1}{2} \frac{v^2 q_{\parallel}^2}{\omega^2} \right) \eta_+(2\mu - \hbar\omega). \quad (8)$$

Upon substituting this form of the polarization function for the monolayer into the integral equation for the inverse dielectric function, we have

$$K(z_1, z_2) = K_{SI}(z_1, z_2) - \sum_{i=1}^N \Pi_{2D,i}^{(0)}(q_{\parallel}, \omega) \int_{-\infty}^{\infty} dz' K_{SI}(z_1, z') v(z' - a_i) K(a_i, z_2). \quad (9)$$

We now set $z_1 = a_i$ in Eq. (9) and obtain

$$\sum_{j=1}^N \left\{ \delta_{jj'} + \Pi_{2D;j}^{(0)}(q_{\parallel}, \omega) \int_{-\infty}^{\infty} dz' K_{SI}(a_{j'}, z') v(z' - a_j) \right\} K(a_j, z_2) = K_{SI}(a_{j'}, z_2). \quad (10)$$

These linear algebraic equations may be solved simultaneously and their solutions expressed in matrix form as

$$\begin{pmatrix} K(a_1, z_2) \\ K(a_2, z_2) \\ \dots \\ K(a_N, z_2) \end{pmatrix} = \frac{1}{S_c^{(N)}(q_{\parallel}, \omega)} \overleftrightarrow{\mathcal{N}}^{(N)}(q_{\parallel}, \omega) \begin{pmatrix} K_{SI}(a_1, z_2) \\ K_{SI}(a_2, z_2) \\ \dots \\ K_{SI}(a_N, z_2) \end{pmatrix}, \quad (11)$$

where $S_c^{(N)}(q_{\parallel}, \omega) = \text{Det} \overleftrightarrow{\mathcal{M}}^{(N)}(q_{\parallel}, \omega)$ with matrix elements given by

$$\mathcal{M}_{jj'}^{(N)}(q_{\parallel}, \omega) = \delta_{jj'} + \Pi_{2D;j}^{(0)}(q_{\parallel}, \omega) \int_{-\infty}^{\infty} dz' K_{SI}(a_{j'}, z') v(z' - a_j) \quad (12)$$

and $\overleftrightarrow{\mathcal{N}}^{(N)}(q_{\parallel}, \omega)$ is the transpose cofactor matrix of $\overleftrightarrow{\mathcal{M}}^{(N)}(q_{\parallel}, \omega)$.

In mean-field theory, we have [25]

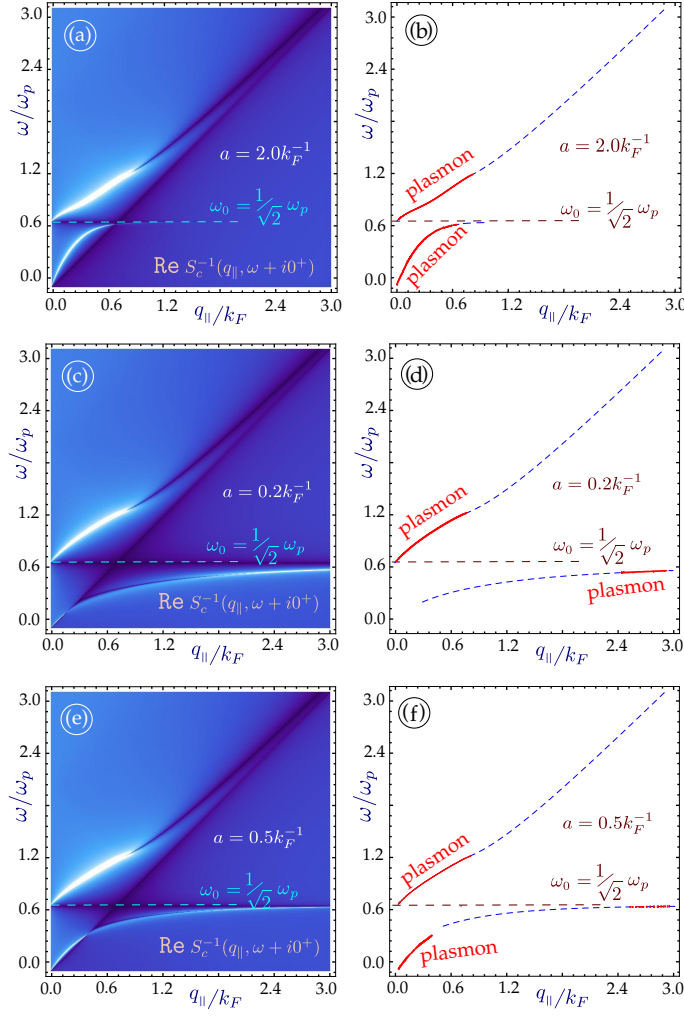


FIG. 1: (Color online) Plasmon dispersion relation for a semi-infinite conductor which is Coulomb-coupled to monolayer graphene for various surface-to-layer separations. In the panels (a), (c) and (e) on the left-hand side, we present density plots of the inverse dispersion function $1/S_c^{N=1}(q_{\parallel}, \omega + i0^+)$ with peaks corresponding to the undamped plasmon modes. The right panels (b), (d) and (f) show numerical solutions for the plasmon branches, both Landau damped and undamped. The distances chosen are $a k_F = 0.2, 1.0$ and 0.5 , correspondingly. All plots are provided for extrinsic graphene (doped) with zero energy bandgap.

$$\begin{aligned}
& K_{SI}(\mathbf{q}_{\parallel}, z, z'; \omega) \\
&= \eta_+(z) \left\{ \delta(z - z') - \frac{\varepsilon(q_{\parallel})}{1 + \varepsilon(q_{\parallel})} e^{-q_{\parallel} z} \delta(z') + \frac{2\varepsilon(q_{\parallel})}{1 + \varepsilon(q_{\parallel})} K_{\infty}^{3D}(\mathbf{q}_{\parallel}, z'; \omega) e^{-q_{\parallel} z} \eta_+(-z') \right\} \\
&+ \eta_+(-z) \left\{ v_{\infty}^{3D}(\mathbf{q}_{\parallel}, z; \omega) \left(\frac{q_{\parallel} \varepsilon(q_{\parallel})}{1 + \varepsilon(q_{\parallel})} \delta(z') - \frac{2q_{\parallel} \varepsilon(q_{\parallel})}{1 + \varepsilon(q_{\parallel})} K_{\infty}^{3D}(\mathbf{q}_{\parallel}, z'; \omega) \eta_+(-z') \right) \right. \\
&\quad \left. + [K_{\infty}^{3D}(\mathbf{q}_{\parallel}, z + z'; \omega) + K_{\infty}^{3D}(q, z - z'; \omega)] \eta_+(-z') \right\}, \tag{13}
\end{aligned}$$

where

$$\varepsilon(q_{\parallel})^{-1} \equiv \frac{2q_{\parallel}}{\pi} \int_0^{\infty} dq_z \left[(q_{\parallel}^2 + q_z^2) \varepsilon_{\infty}^{3D}(\mathbf{q}, \omega) \right]^{-1}, \tag{14}$$

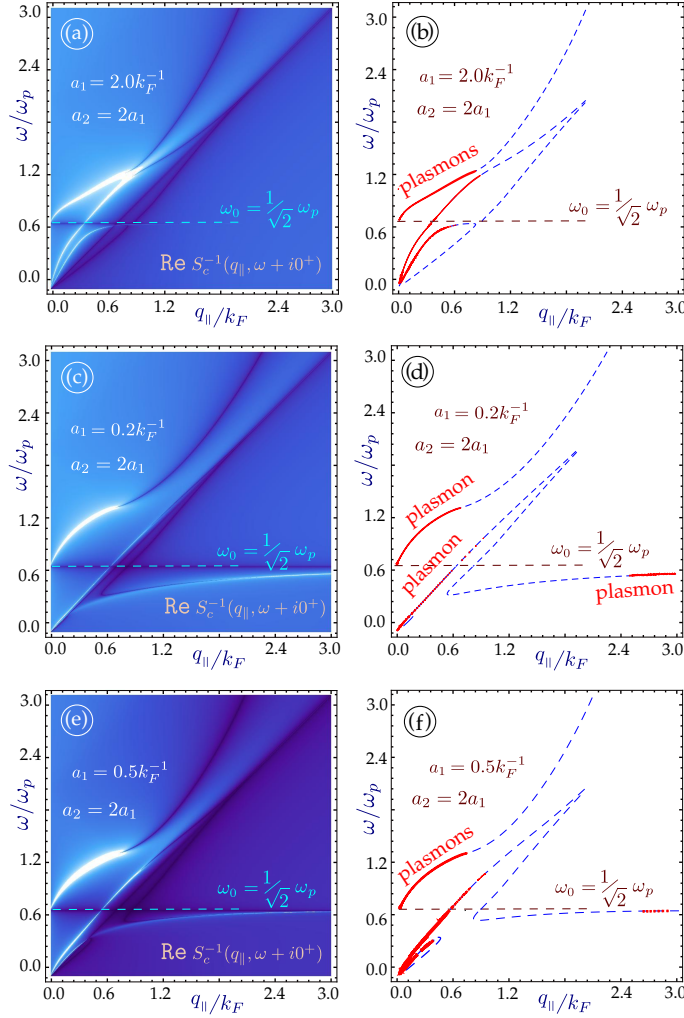


FIG. 2: (Color online) Plasmon excitation spectra for a semi-infinite conductor interacting through the Coulomb interaction with $N = 2$ monolayer graphene sheets located at chosen distances from the surface. The left-hand panels (a), (c) and (e) give density plots of the inverse dispersion function $1/S_c^{N=2}(q_{\parallel}, \omega + i0^+)$ with peaks corresponding to the plasmon modes. The right panels (b), (d) and (f) show the numerical solutions for the Landau damped (dashed blue lines) and undamped (red curves) plasmon branches. The plots show results for various distances between the surface and the layers: $a_1 k_F = 2.0, 0.2$ and 0.5 , respectively. The second layer is placed at a distance a_2 , equal to twice as large as a_1 . All the plots are provided for extrinsic graphene (doped) with zero energy bandgap.

and $\epsilon_{\infty}^{3D}(\mathbf{q}, \omega)$ denotes the three dimensional (3D) bulk dielectric function of the thick-slab material. Furthermore, Eq. (13) introduces the definitions

$$K_{\infty}^{3D}(q_{\parallel}, z'; \omega) = \frac{1}{\pi} \int_0^{\infty} dq_z \frac{\cos q_z z'}{\epsilon_{\infty}^{3D}(\mathbf{q}, \omega)} \quad (15)$$

and

$$v_{\infty}^{3D}(q_{\parallel}, z'; \omega) = \frac{2}{\pi} \int_0^{\infty} dq_z \frac{\cos q_z z'}{(q_{\parallel}^2 + q_z^2) \epsilon_{\infty}^{3D}(\mathbf{q}, \omega)} . \quad (16)$$

Making use of these results in Eq. (11), we then obtain

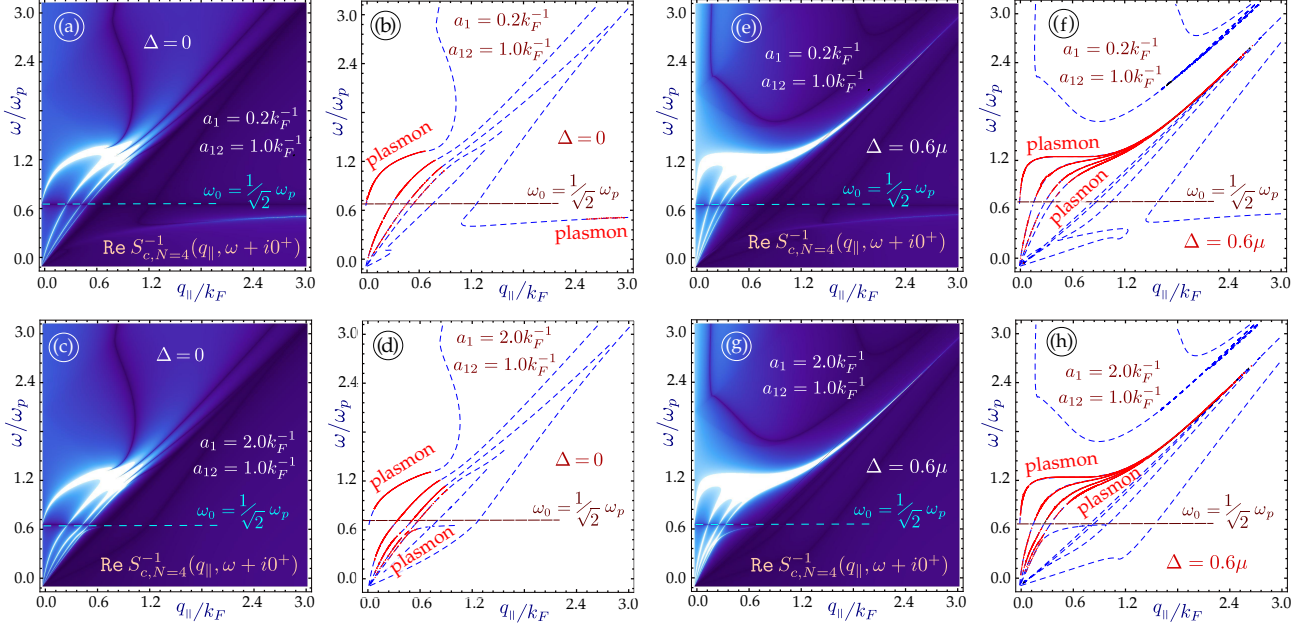


FIG. 3: (Color online) Density plots showing the bulk modes in the miniband continuum and the line traces of plasmon dispersion for $N = 4$ graphene layers on a conducting substrate. The line plots show damped (dashed blue lines) and undamped (red curves) plasmon excitations. In (a)-(d), the layers are gapless, and in (e)-(h) each layer has a gap $\Delta = 0.6 \mu$. The layers are equally spaced with inter-layer spacing $a_{12} = k_F^{-1}$. The separation between the first layer and the surface was chosen as $a_1 k_F = 2.0$ $a_1 k_F = \mu/\hbar v_F$. If the gap or number of layers is increased, the lowest branch does not re-appear for large q_\parallel . It is more complicated than we thought.

$$\begin{aligned} \mathcal{M}_{jj'}^{(N)}(q_\parallel, \omega) &= \delta_{jj'} + \frac{2\pi e^2}{\epsilon_s q_\parallel} \Pi_{2D;j}^{(0)}(q_\parallel, \omega) \left[e^{-q_\parallel |a_j - a_{j'}|} + e^{-q_\parallel (a_j + a_{j'})} \frac{\varepsilon(q_\parallel)}{1 + \varepsilon(q_\parallel)} \right. \\ &\quad \left. + \frac{2\varepsilon(q_\parallel)}{1 + \varepsilon(q_\parallel)} e^{-q_\parallel a_j} \int_0^\infty dz' e^{-q_\parallel |z' - a_j|} K_\infty^{3D}(q, z'; \omega) \right]. \end{aligned} \quad (17)$$

If the bulk plasma within the semi-infinite slab is fully local in the sense that $\epsilon_\infty^{3D}(\mathbf{q}, \omega) \rightarrow \equiv \varepsilon_B(\omega) = 1 - \omega_p^2/\omega^2$, in terms of the bulk plasma frequency ω_p , then we use

$$\begin{aligned} K_\infty^{3D}(q, z'; \omega) &= \frac{\delta(z')}{\varepsilon_B(\omega)} \\ v_\infty^{3D}(q_\parallel, z'; \omega) &= \frac{e^{-q_\parallel |z'|}}{q_\parallel \varepsilon_B(\omega)} \end{aligned} \quad (18)$$

from which the corresponding local inverse dielectric function $K_{ST}^{local}(\mathbf{q}_\parallel, z, z'; \omega)$ may be obtained using Eq. (13).

While Eq. (17) is useful because of its apparent simplicity, it is necessary to understand that its validity is restricted because the q_z -integrations in Eqs. (14 through 16) extend over an infinite integration range. This blends the effects of the boundary/image length scale with that of the q_z -nonlocality dependence, eliminating the possibility of an unrestricted limit $q_z \rightarrow 0$ and modifying the plasmon dependence on q_\parallel . Additionally, the imaginary part of $\varepsilon_\infty^{3D}(\mathbf{q}, \omega)$ is accounted for in these q_z -integrations, which consequently contributes to damping of the surface plasmon modes even in the low- q_\parallel limit. The "nonlocal" q_\parallel -correction to the surface plasmon, and its imaginary part involving damping, depend on the properties of the bounding surface. But, there is a range of applicability. This can be seen by examining the parameter measuring the importance of nonlocality in the bulk dielectric function $\varepsilon_\infty^{3D}(\mathbf{q}, \omega)$, namely $p_c^M \sim (m^* \omega_p^2 / E_{thermal})^{1/2}$, where the characteristic thermal energy $E_{thermal} = \mu$ is the Fermi energy in the degenerate substrate with electron effective mass m^* . For $q_\parallel \ll p_c^M$, it is reasonable to neglect nonlocality, at least in the surface plasmon frequency $\omega_s = \omega_p / \sqrt{2}$ as well as in comparison with other more pertinent sources of nonlocal behavior (but it cannot be neglected in the damping of the surface plasmon).

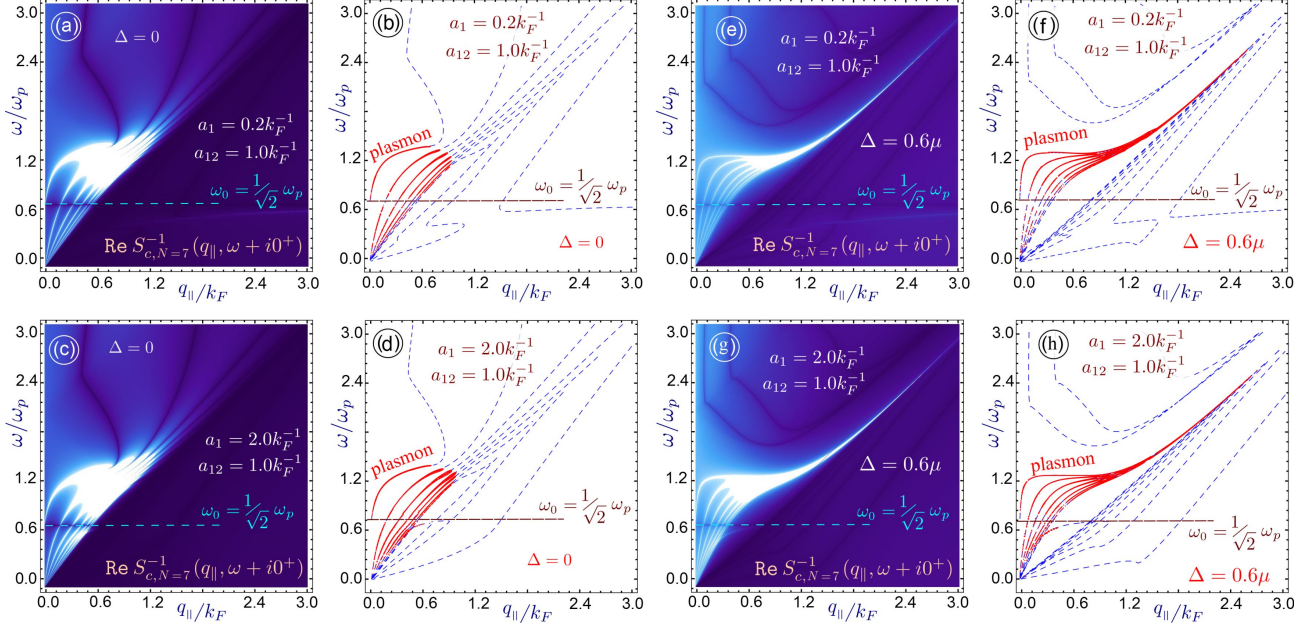


FIG. 4: (Color online) Plasmon dispersion for $N = 7$ graphene layers on a conducting substrate. As in Fig. 3, the layers in (a)-(d) are gapless, whereas in (e)-(h) each layer has a gap $\Delta = 0.6 \mu$. The inter-layer separation is $a_{12} = k_F^{-1}$. The first layer is at distances $a_1 k_F = 0.2$ from the surface of the semi-infinite conductor. If the gap or number of layers is increased, the lowest branch does not re-appear for large q_\parallel .

III. NUMERICAL RESULTS

In this section, we present numerical results for the plasmon dispersion for a system consisting of a semi-infinite conducting medium which is Coulomb coupled to $N = 1, 2, 4$ layers of graphene as shown in Figs. 1 through 4. We note that both the plasmon solutions and damping by bulk modes in the miniband continuum crucially depend on the separation between the constituents as well as the energy gap between the valence and conduction bands. For a single layer, our results shown in Fig. 1 demonstrate that if the plasmon mode enters a region with $\text{Im } \Pi_{2D}^{(0)}(q_\parallel, \omega) \neq 0$, the mode is Landau damped. Our calculations also show that when the distance a is less than a critical value $d_c \simeq 0.4 k_F^{-1}$, in terms of the Fermi wave vector $\mu/\hbar v_F$, the lower acoustic plasmon mode is over-damped and this behavior seems analogous to data reported experimentally [9–13]. This is obviously the case if the plasmon branch goes below the main diagonal $\omega = v_F q_\parallel$. The damping, as well as the critical distance changes in the presence of an energy bandgap for graphene.

Similar conclusions for a pair of graphene layers electrostatically coupled to a semi-infinite conducting material are presented in Fig. 2. The principal difference between the case when there are two Coulomb-coupled layers is that if the distance of the layer nearest the conductor is less than the critical separation d_c , both symmetric and antisymmetric modes become damped, for different ranges of wave vector. We emphasize that the upper plasmon branch (symmetric mode) remains almost unchanged for all cases, either with one or two graphene layers.

The role played by the energy band gap is an important part of our investigation. For monolayer graphene, an energy gap leads to an extended region of undamped plasmons [26]. As we mentioned before, we pay particular attention to the regions outside of the single-particle excitation continuum with $\text{Im } \Pi_{2D}^{(0)}(q_\parallel, \omega) = 0$, since the plasmons

in these regions are not Landau-damped. In Figs. 3 and 4, we have plotted the plasmon dispersion relation for $N = 4$ and $N = 7$ graphene layers without and with an energy bandgap as well as for various distances between the nearest layer to the conducting surface. These results show that for a conducting substrate surface plasmon frequency denoted by $\omega_s = \omega_p/\sqrt{2}$, the surface plasmon frequency ω_c of the hybrid superlattice always lies below ω_s . Furthermore, the intensity of this mode depends on the distance of the graphene layers from the surface of the conductor as well as the energy band gap between the valence and conduction bands of MLG. In the absence of a gap, our calculation shows that when the conductor surface-MLG separation exceeds a critical distance d_c , the intensity of the surface plasmon in the long wavelength regime is high and may be detected up to some cut-off wave vector q_c . For $q_{\parallel} > q_c$, the intensity of ω_c is very weak until the plasmon wave vector exceeds some value q'_c . However, when the surface-MLG separation is less than d_c , the surface plasmon intensity in the long wavelength regime is weak and the mode only appears at shorter wavelength when $q_{\parallel} > q'_c$. For gapped graphene, the surface plasmon frequency ω_c is completely suppressed when the surface-layer separation is less than d_c .

IV. CONCLUDING REMARKS

The appearance of a surface plasmon polariton for a multi-layer structure consisting of 2DELs was predicted in the 1980's by Giuliani and Quinn [2] as well as by Jain and Allen [3]. This surface mode is free from Landau damping or damping by bulk modes in the miniband continuum and lies "above" the continuum of bulk modes. Additionally, this surface mode only exists above a critical wave vector q_{\parallel}^* which is determined by the layer spacing and the difference in the background dielectric constants of the layers and the surrounding medium. When q_{\parallel}^* , there is damping by the bulk plasmon modes. As a matter of fact, the dispersion equation for the layered superlattice structures investigated in [2, 3] is a special case which may be obtained from our more general Eq. (17) where we included the effects arising from a substrate.

Very recently, in a series of experiments to determine the nature and behavior of plasmon excitations in graphene interacting with metallic substrates, Politano, et al. [9–12] showed how the dispersion and intensity may be affected in a substantial way. The experimental results show that self-doped graphene supported by a metal substrate has two plasmon branches. There is an acoustic plasmon, with a linear dispersion, and a nonlinear plasmon. Both plasmon branches are similar in nature to those we presented in Fig. 1, originating from the presence of a substrate. The present paper investigating the effects of a substrate on the plasmon excitations in a superlattice of graphene was stimulated by the experimental results on supported graphene. We are aware of the theoretical work on free-standing superlattice structures of MLGs [7], but the results there do not address the coupling to a metallic substrate which drastically affect the plasmon dispersion relation as may be observed from Figs. 1 through 2.

The important conclusions of our work are as follows. We formulated and exploited a newly derived expression for plasmon dispersion in a superlattice of 2D layers which are Coulomb-coupled to a metallic substrate by taking into account the full nonlocality of the layers as well as the underlying conductor. We predict the existence of low-frequency nonlocal plasmon excitations at the vacuum-surface interface for various conditions of surface-layer separation as well as the energy gap. When the separation between the conducting surface and the nearest layer is less than some critical distance d_c , the surface plasmon may not exist in the long wavelength limit. We obtain a surface plasmon at both intermediate as well as long wavelengths as this layer-surface separation is increased. For this hybrid structure, the surface plasmon frequency lies below the surface plasmon frequency for the semi-infinite substrate. Experimental verification of these simulated results may be achieved using high-resolution electron-energy-loss spectroscopy (EELS) [27], for example. This paper was inspired by recent experimental work investigating the effect due to a metal on the collective plasmon mode of a single layer of graphene [9, 10]. We presented a new approach for generating a tunable surface plasmon using hybrid semiconductors. Additionally, our proposed approach based on hybrid semiconductors can be generalized to include other novel two-dimensional materials, such as hexagonal boron nitride, molybdenum disulfide and tungsten diselenide.

Acknowledgments

This research was supported by contract # FA 9453-13-1-0291 of AFRL.

[1] G. A. Sai-Halasz, R. T. Tsu, and L. Esaki, Applied Phys. Lett. **30**, 651 (1977).

- [2] G. F. Giuliani and J. J. Quinn, Phys. Rev. Lett. **51**, 919 (1983).
- [3] J. K. Jain and P. B. Allen, Phys. Rev. Lett. **54**, 2437 (1985).
- [4] N. J. M. Horing and J. D. Mancini, Phys. Rev. B **34**, 8954 (1986).
- [5] A. C. Tles and J. J. Quinn, Phys. Rev. B **29**, 2021 (1984).
- [6] G. Gumbs and M. K. Ali, Phys. Rev. Lett. **60**, 1081 (1988).
- [7] J.-J. Zhu, S. M. Badalyan, and F. M. Peeters Phys. Rev. B **87**, 085401 (2013).
- [8] Giovanni Bertoni, Lionel Calmels, Anne Altibelli, and Virginie Serin, Phys. Rev. B **71**, 075402 (2004).
- [9] A. Politano, A. R. Marino, V. Formoso, D. Far?as, R. Miranda, and G. Chiarello, Phys. Rev. B **84**, 033401 (2011).
- [10] A. Politano, A. R. Marino, and G. Chiarello, Phys. Rev. B **86**, 085420 (2012).
- [11] A. Politano, and G. Chiarello, Applied Physics Letters, **102**, 201608 (2013).
- [12] A. Politano, and G. Chiarello, Nanoscale, **5**, 82158220. (2013).
- [13] C. Kramberger, R. Hambach, C. Giorgetti, M. H. Rmmeli, M. Knupfer, J. Fink, B. Bchner, Lucia Reining, E. Einarsson, S. Maruyama, F. Sottile, K. Hannewald, V. Olevano, A. G. Marinopoulos, and T. Pichler, Phys. Rev. Lett. **100**, 196803 (2008).
- [14] A. M. Shikin, D. Faras, V. K. Adamchuk, and K.-H. Rieder, Surf. Sci. **424**, 155 (1999).
- [15] Hu Zi-pu, D. F. Ogletree, M. A. Van Hove, and G. A. Somorjai, Surf. Sci. **180**, 433 (1987).
- [16] T. Aizawa, R. Souda, S. Otani, Y. Ishizawa, and C. Oshima, Phys. Rev. B **42**, 11469 (1990).
- [17] O. V. Kibis Phys. Rev. B **81**, 165433 (2010).
- [18] Andrii Iurov, Godfrey Gumbs, Oleksiy Roslyak, and Danhong Huang, Journal of Physics: Condensed Matter **24**, 015303 (2012).
- [19] C. W. Chiu, F. L. Shyu, M. F. Lin, Godfrey Gumbs, and Oleksiy Roslyak, J. Phys. Soc. Jpn. **81**, 1047 03 (2012).
- [20] Godfrey Gumbs, Andrii Iurov, and N. J. M. Horing, Phys. Rev. B **91**, 235416 (2015).
- [21] B Wunsch, T Stauber, F Sols, and F Guinea, New J. Phys. **8**, 318 (2006).
- [22] P. K. Pyatkovskiy, J. Phys.: Condens. Matter **21**, 025506 (2009).
- [23] K. W.-K. Shung, Phys. Rev. B **34**, 1264 (1986).
- [24] E. H. Hwang and S. DasSarma, Phys. Rev. B **75**, 205418 (2007).
- [25] N. J. M. Horing, Elliott Kamen, and Hong-Liang Cui, Phys. Rev. B **32**, 2184 (1985).
- [26] P. K. Pyatkovskiy, J. Phys.: Condens. Matter **21**, 025506 (2009).
- [27] S. Y. Shin, N. D. Kim, J. G. Kim, K. S. Kim, D. Y. Noh, Kwang S. Kim, and J. W. Chung, Appl. Phys. Lett. **99**, 082110 (2011).